Remote Sensing of Environment 114 (2010) 1765–1776

Contents lists available at ScienceDirect

Remote Sensing of Environment

journal homepage: www.elsevier.com/locate/rse

Synoptic mapping of internal-wave motions and surface currents near the Lombok Strait using the Along-Track Stereo Sun Glitter technique

J.P. Matthews [a,b,*], T. Awaji [a]

[a] Department of Geophysics, Kyoto University, Kyoto, Japan
[b] Environmental Satellite Applications, Llys Awel, Mount Street, Menai Bridge, Anglesey, Wales, United Kingdom

ARTICLE INFO

Article history:
Received 7 September 2009
Received in revised form 18 February 2010
Accepted 10 March 2010

Keywords:
Along-Track Stereo
Sun Glitter
PRISM
ASTER
Internal waves
Surface currents
Lombok Strait

ABSTRACT

A multi-component satellite remote sensing program is required to track the response of the world's oceans, lakes and rivers to climate change. Central to this endeavor is the ability to detect the motions of internal waves, swell waves and currents and hence follow energy transport and exchange. However, the present methods of monitoring the motions of water bodies from space, such as those based on altimetry or gravity measurements, are geared mostly toward applications on large spatial scales, whereas the capacity to map the fine details of hydrospheric flows is limited. This paper describes a satellite-based method of detecting wave motion and surface currents at high (in principle metric) resolution that can be applied under specific circumstances in the confined environs of narrow sea straits, lakes and rivers and that compliments the use of other high-spatial resolution techniques such as those based on Synthetic Aperture Radar (SAR). The Along-Track Stereo Sun Glitter (ATSSG) technique makes use of images of water bodies that are separated in time by roughly 1 min and are gathered in the forward-, nadir- and backward-looking directions by space-borne optical sensors performing along-track observations. When sensor viewing geometries lead to the presence of Sun glitter in these images, surface slicks, internal waves, swell waves and other phenomena become highlighted through the surface roughness changes they induce, since these in turn modulate the reflected glitter radiance. Measurement of the differential displacements between congruent sections of the surface roughness signatures present within image pairs of the stereoscopic sequence then enables internal wave or swell wave motions to be determined, while surface currents can be deduced if "passive" tracers of the flow in the form of surface roughness structures (such as slicks) are present. The application of the ATSSG technique described herein makes use of data acquired at a spatial resolution of 2.5 m by the Panchromatic Remote-sensing Instrument for Stereo Mapping (PRISM) to provide the first along-track fine-scale synoptic mapping of the surface motions of individual components within a large group of internal waves and to generate supporting surface-current measurements. The PRISM data we employ were acquired to the south of the Lombok Strait (Indonesia), where highly energetic internal-wave growth takes place and where through-flow surface-current data, of the type derived by the ATSSG technique, can be of value in climate studies.

1. Introduction

A limitation of present oceanographic satellite remote sensing techniques lies in their inability to measure the surface velocities of waves and currents at high-spatial resolution (defined here nominally as <100 m). For currents, this restriction is generally of little concern when issues relating to the open ocean are under consideration, since then motions can be deduced by other techniques such as satellite altimetry (Fu & Chelton, 1985), the tracking of surface temperature patterns (Turiel et al., 2008) or, on yet larger scales, the deduction of mass movements from changes in the earth's gravity field (Ponte & Quinn, 2009). However, important components of the hydrosphere involve water movements through, and wave generation within, spatially narrow zones such as sea straits, lakes and rivers. In these cases, techniques for remotely sensing wave and current motions at high-spatial resolution are required. This need is particularly acute in the vicinity of narrow sea straits such as the Lombok Strait of Indonesia or the Strait of Gibraltar where, in spite of the physical restrictions, exchanges of global significance linking diverse oceanographic regimes take place and where powerful internal waves arise. A similar requirement for detailed monitoring exists in the channels and estuarine zones associated with major rivers such as the Amazon, which are likewise relatively small on oceanic scales, but which nevertheless impart large influences on terrestrial and marine environments.

* Corresponding author. Environmental Satellite Applications, Llys Awel, Mount Street, Menai Bridge, Anglesey, Wales, United Kingdom.
E-mail address: johnp_matthews@hotmail.com (J.P. Matthews).

0034-4257/$ – see front matter © 2010 Elsevier Inc. All rights reserved.
doi:10.1016/j.rse.2010.03.007

In parallel with the need for fine-scale remote sensing of surface currents, an ability to make high-spatial resolution measurements of the surface propagation characteristics of internal waves from space is also necessary, since these disturbances represent important dynamical constituents of aquatic environments (Garrett & Munk, 1979) due to their key role in generating ocean turbulence (Alford, 2003). In terms of simple theory, internal waves are established at, and propagate along, density interfaces within the stratified regimes of oceans and lakes. Research has demonstrated that these common disturbances are able to transmit energy over considerable distances and that they produce significant biological and dynamical impacts through the mixing they induce (Haury et al., 1979; Wunsch & Ferrari, 2004). For swell waves, which share some of these properties, detailed phase speed data coupled with surface-current information can provide a useful platform for oceanographic research, particularly for coastal zones threatened by sea level rise and the erosion it may engender (Zhang et al., 2004).

Recent research has sought to improve the monitoring of ocean dynamics. Sea surface height measurements to be provided by planned altimeter missions will provide a fine mesh for the retrieval of surface and deep ocean circulations on a range of scales down to about 20 km (Klein et al., 2009). Progress has also been made in surface-current measurement using satellite SAR systems (Chapron et al., 2005; Goldstein & Zebker, 1987), and most recently to provide line-of-sight current information at spatial resolutions of around 5 km (Johannessen et al., 2008). In addition, Romeiser et al. (2005) have reported Shuttle-based interferometric SAR (INSAR) current determinations in the Dutch Wadden Sea and later in the German Elbe River (Romeiser et al., 2007) with an effective resolution of around 1 km. These SAR-based techniques represent a highly promising approach to the measurement of aquatic surface motions from space and have the advantage of offering an all weather, day/night operability. Furthermore, resolutions of about 100 m should be theoretically possible with future along-track INSAR data from TerraSAR-X (Romeiser & Runge, 2007). However, none of these techniques can at present deliver surface-current vectors at spatial resolutions of 100-m or better.

The measurement of internal-wave motions on fine spatial scales has received generally less attention, although recent research by Zhao et al. (2008) obtained motion data at about 150 m resolution by exploiting a rather atypical opportunity offered by tandem SAR imaging, with sensors mounted on two satellites following similar orbital paths and separated in time by 28 min. Nonetheless, the mapping of internal-wave motions over sub-minute timescales from a single along-track imaging system has not so far been reported.

In this article, we suggest that future applications of both the altimeter- and SAR-based methods of oceanic motion determination could be strengthened through the simultaneous use of a technique based on optical measurements. Under appropriate imaging conditions, this provides accurate surface motion data at very high-spatial resolution and thus offers a means of calibration and inter-comparison. Termed the Along-Track Stereo Sun Glitter (ATSSG) technique, it determines vector currents and internal- and gravity-wave velocities by measuring the displacements of Sun glitter signatures gathered (ideally) in the "triplet" of forward-, nadir- and backward-looking directions by along-track stereoscopic devices. Given the reliance on passive optical observations, this necessarily takes place under the more restrictive conditions (relative to those for radar-based approaches) of low percentage cloud cover during daytime and low to moderate winds. For current measurements, the method is also limited by the requirement that roughness structures in the form of slicks must be present on the ocean surface. Clearly, the fact that Sun glitter signatures from slicks or waves must be present in at least two of the images of the along-track acquisition also constrains the applicability of the technique when data from sensors designed for land-based research are used. The aim of this article is to show that, in spite of these restrictions, the ATSSG approach remains a useful diagnostic tool in the study of waves, currents and fronts and that it can potentially strengthen the interpretation of remotely sensed water motion data determined simultaneously by radar techniques.

When the earth's oceans and lakes are viewed from space, the surface impressions of many complex aquatic and atmospheric dynamical processes become accentuated in bright areas of Sun glitter (Apel et al., 1975; Cox & Munk, 1954; Hennings et al., 1994; Munk et al., 2000). This highlighting stems from the fact that the reflected Sun glitter radiance depends on the small-scale textural roughness of the ocean (or lake) surface. The latter, formed from wavelets in the capillary and short-gravity-wave regimes, responds to the presence of surfactant slicks and to the current and wind systems established near the surface. In this sense, the factors governing the reflected Sun glitter radiance resemble those for SAR backscatter, although in the case of radar the influence of the wavelength of the system, in particular, must be borne in mind (Matthews et al., 1997). Many of the hand-held photographs of oceanic internal waves, spiral eddies, fronts and other phenomena acquired by astronauts since the early days of manned space exploration have been obtained within the Sun glitter regime (a selection of which can be viewed online at the image gallery maintained by the Johnson Space Center). Although such data are testimony to the fact that Sun glitter "opens a window" on the ocean to reveal some of its inner workings, it is well known that great care is needed in their interpretation.

Unmanned satellite-borne optical sensors also provide synoptic views across large oceanic regions covered by Sun glitter when their observational geometries permit. A good example of the broad geographical applicability of satellite Sun glitter data is given in the recent survey performed by Jackson (2007), in which the author recorded numerous internal-wave glitter events occurring over a wide range of latitudes (between about 55°N and 45°S). These events were detected between August 2002 to May 2004 by the Moderate Resolution Imaging Spectroradiometer (MODIS, spatial resolution = 250 m) carried on the Terra and Aqua spacecraft. The latitudinal range of these internal-wave detections at any specific time of year generally covered about 55° and followed the movement of the changing location of the Sun glitter regime, shifting northward to maximum extent during boreal summer to cover a range that was roughly delimited by the equator and the 55°N line. Jackson (2007) demonstrated that the internal-wave events became apparent within large swaths of Sun glitter that cover substantial portions of the 2300-km swath of MODIS. Comparable Sun glitter surveys have not so far been performed for the narrower-swath optical sensors discussed in this article, in part because of their less systematic coverage, although on the basis of anecdotal evidence gathered so far, it is apparent that the summer season is best suited for Sun glitter imaging away from the equator in these cases also.

To date, the stereoscopic satellite Sun glitter data required for ATSSG applications have been gathered fortuitously as "spin-offs" from missions that are aimed primarily toward topographic mapping. Hence, owing to the non-targeted nature of the data source, the supply of high-spatial resolution data suitable for use in ATSSG mapping is limited. However, given the importance of surface-current and wave speed determinations as input data for new climate models, it is hoped that the present paper will help to stimulate interest in a more dedicated approach to the acquisition of Sun glitter data from space.

This article considers remote sensing issues that are relevant to aquatic applications of stereoscopic satellite data, while questions relating to the seasonal and oceanographic aspects of the detected internal-wave and surface-current fields will be dealt with in other submissions. The work begins with a brief historical review of ATSSG progress so far. This is followed by a basic description of the Lombok Strait, which separates the islands of Bali and Lombok (Indonesia), from where the PRISM data used in this study were acquired. The paper then considers some fundamentals of the imaging of internal waves in order to better interpret these PRISM data. The twin aspects of internal-wave motion determination and surface-current mapping are then discussed, particularly with a view to highlighting some obvious drawbacks of the ATSSG technique and, on the other hand, to suggest new areas of application in the study of wave refraction and in frontal research. In the summarizing comments, we discuss aspects that are germane to the continued development and validation of the ATSSG technique as a means of remotely sensing the dynamical aspects of marine and freshwater environments at high-spatial resolution.

2. Development of the ATSSG technique

Earlier work (Matthews et al., 2004) established the principle underpinning the ATSSG method through the chance discovery that space-borne optical sensors acquiring along-track stereo image sequences primarily for topographic applications occasionally capture multiple views of Sun glitter patterns when operating over water bodies. These authors presented images acquired by the Visible and Near Infra-Red (VNIR) sub-component of the Advanced Space-borne Thermal Emission and Reflection Radiometer (ASTER) that revealed highly structured Sun glitter features from pristine Lake Nam Co, Tibet, in both the nadir view (channel 3N) and in the backward-looking view (channel 3B) gathered some 55 s later from a slanted viewing direction. As a result of the specific viewing geometry of the VNIR sensor, the glitter features in channel 3B were brightness “flipped” in appearance relative to the nadir signature and hence the term “Region of Brightness Reversal” (ROBR) was later coined to describe areas exhibiting this effect.

A subsequent paper (Matthews, 2005) considered the geometrical requirements for Sun glitter viewing within an along-track stereo configuration and noted the presence of internal-wave signatures in both the nadir and back-looking ASTER views. This paper also presented the first ATSSG surface-current determinations, which in this case defined the motion of an extensive ship wake. Although the comparison was limited in extent, the results obtained corresponded favorably with surface-current determinations made by high-frequency (HF) radar, a shore-based ocean surface remote sensing technique that has now gained widespread acceptance (Barrick et al., 1977; Matthews et al., 1993; Prandle & Matthews, 1990; Yoshikawa & Masuda, 2009). It was noted that the ATSSG method provides an exact method of surface-current determination in the sense that it measures a differential displacement that develops over a specified time interval and is not reliant on heavy averaging or on factors such as the motion of rotor blades or on a specific interpretation of back-scattered wave spectra.

In this early work, it was soon realized that ASTER stereoscopic data were far from ideal for use in the ATSSG differential approach since, even in the best case of a target with a distinct outline that can be unambiguously identified in adjacent views, data at 15-m spatial resolution and with a 55 s time delay between the nadir and slant acquisitions lead to internal-wave speed estimates and surface-current determinations at a relatively coarse resolution of 0.27 m s^{-1}. As a response, in part, to this limitation, the focus then turned towards the application of ASTER data in the study of quasi-stationary features visible in glitter, such as the surface roughness signatures created by stratified flows over bottom topography (Matthews et al., 2008).

However, a new research opportunity arose with the availability of data from the Panchromatic Remote-sensing Instrument for Stereo Mapping (PRISM), which became operational in 2006 with the launch of the Advanced Land Observing Satellite (ALOS) platform (Igarashi, 2001). This device makes panchromatic (520–770 nm) along-track observations in the forward, nadir and backward-looking directions from telescopes tilted at angles close to nominal values of +24°, 0° and −24° relative to nadir. Since the PRISM image triplets are gathered at a spatial resolution of 2.5 m and the component images within the sequence are each separated in time by 45.3 s, the resolution in speed now becomes ideally 5.5 cm s^{-1} (again, assuming precise feature correspondence), which represents a considerable improvement in performance relative to ASTER.

In practice, the actual resolution in surface-current determination will be coarser than these estimates due to the influence of a range of factors such as co-registration inaccuracies, inter-view residuals and effects that may relate to the evolution of the internal-wave field or to the change in viewing geometry. In addition, for surface-current determinations, the synoptic resolution (i.e. the spatial coverage of the motion vectors) will depend on the distribution of ambient surface roughness features and hence is non-uniform, in contrast to the more systematic data-mapping capability of radar methods. In order to provide a platform for a discussion of the practical issues and difficulties involved in the application of the ATSSG approach, the present paper analyzes high quality PRISM data in an ATSSG-based study of internal-wave motions and surface currents observed in and around the Lombok Strait of Indonesia.

3. The Lombok Strait study region

The Lombok Strait (Fig. 1) offers one of several major arterial links between the tropical Pacific and Indian Oceans. It represents a vital component in the global circulation system, since it carries roughly 25% of the Indonesian Throughflow (ITF) current (Murray & Arief, 1988) and is thereby the conduit for a substantial heat flux into the Indian Ocean. The factors influencing the variability of Lombok Strait throughflow have been much discussed (e.g. Wyrtki, 1987; Gordon, 2005) and are of prime interest for studies of inter-ocean energy exchange and its consequent influences on climate. During the boreal summer and early autumn months relevant to this study, the active southeast monsoon establishes a well-defined southward residual flow through the Lombok Strait that is strongest in the main channel between Nusa Penida and Lombok islands (Fig. 1). Residual flows during the northwest monsoon of boreal winter become generally more variable and may reverse northward in response to specific wind forcing events (Arief & Murray, 1996). There is also a relation between the throughflow and the El Niño Southern Oscillation (ENSO) (Meyers, 1996).

In spite of their considerable oceanographic and climatological significances, the currents through the Lombok Strait have been relatively little studied by direct means. On the other hand, indirect methods, such as the deduction of geostrophic flows from pressure-gauge measurements (Chong et al., 2000; Sprintall et al., 2004), have had greater though still not extensive usage. Recent work (Sprintall et al., 2009), however, has provided full-depth velocity measurements from moorings in the Lombok Strait and elsewhere in the ITF region. The use of *in situ* instrumentation in this way is difficult in the sill region between Nusa Penida and Lombok islands, since there the currents can be rapid (up to 3.5 m s^{-1}). In addition, the busy shipping and fishing traffic coupled with other constraints has tended to restrict data acquisition by this means and by ship-based Acoustic Doppler Current Profiler (ADCP) measurements. In principle therefore, the Lombok Strait presents an ideal opportunity for the application of a remote sensing approach to surface-current determination and one which, given the scientific importance of the through-flow, should be addressed with some urgency. However, the narrow confines of the passage and the inherent limitations of spatial resolution have meant that neither altimetry nor SAR-based methods have been able to deliver the fine-scale flow information required to study the details of the transport and thereby shed light on this branch of the ITF.

A shortage of surface motion measurements also hinders studies of the region's powerful (oceanic) internal waves. The rapid flows of

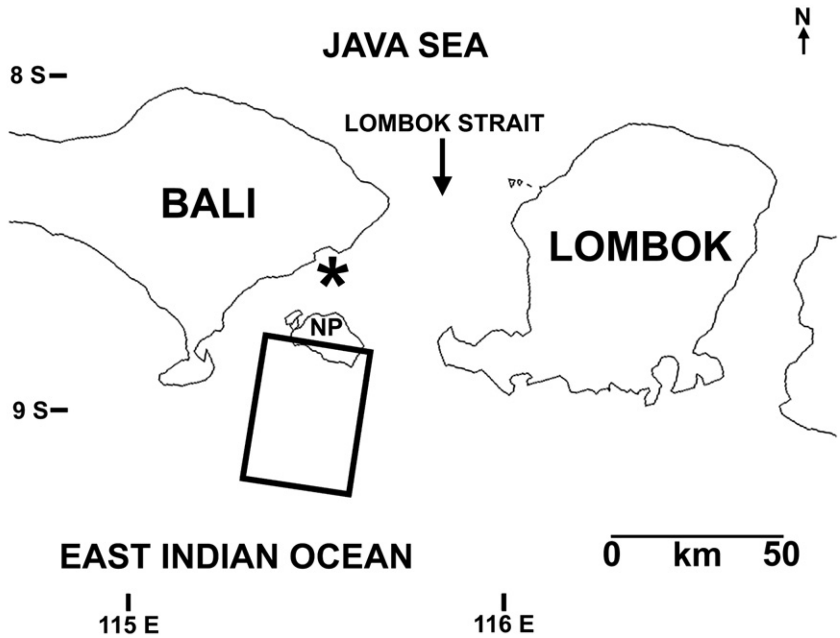

Fig. 1. Map of the Lombok Strait study region. The black arrow indicates the largely southward through-flow current established during the southeast monsoon. The region enclosed by the rectangle represents the area presented in Fig. 2, while the black star marks the location of the data presented in Fig. 8. NP denotes the island of Nusa Penida.

water over the topographic sill of the Lombok Strait, together with the sharp density contrasts present in these waters, lead to the generation of strong internal waves, which transmit energy over great distances and, in so doing, work to mix the surrounding waters by establishing circulation systems that operate down to depths of about 1500 m. The disturbances originating from the Lombok Strait propagate outwards from both ends of the passage (i.e. northward into the Java Sea and southward into the East Indian Ocean). They represent some of the most powerful internal waves observed on earth and are capable of transmitting around 1 GJ of energy per meter length of wave front. Previous work on these internal waves has generally relied on SAR imaging (Mitnik et al., 2000; Susanto et al., 2005), with wave phase speeds deduced indirectly by measurement of the distance between successive internal-wave packets generated on adjacent semi-diurnal tides. Given their considerable regional significance, it is appropriate that these Lombok Strait disturbances should form the subject of the first synoptic ATSSG mapping of internal-wave motions.

4. PRISM Sun glitter imaging of Lombok Strait internal waves

Fig. 2 presents a portion of the region imaged by PRISM at 10.41 LT on 26 September 2006 (toward the end of the southeast monsoon) and covers the region outlined by the black rectangle in Fig. 1. On this date, the nadir and backward-looking views of the sensor provided

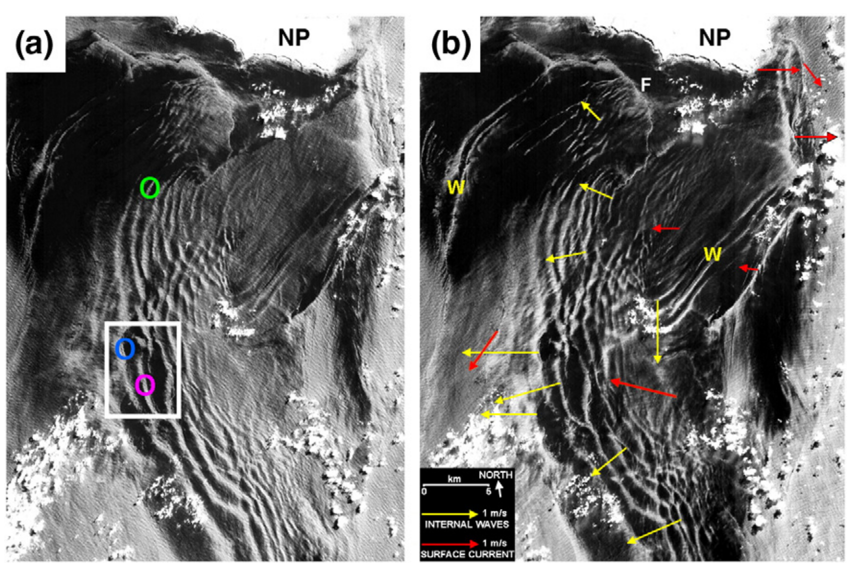

Fig. 2. (a) Nadir PRISM data acquired at 02.41.09 UT (10.41 LT) on 26 September 2006 depicting the area enclosed by the rectangle in Fig. 1. Braided internal-wave Sun glitter signatures to the south of Nusa Penida (NP) are indicative of the presence of multiple wave sources. The small purple (blue and green) ring indicates the source region of the data presented in Fig. 4 (Figs. 6 and 7), while the white rectangle encloses the region depicted in Fig. 5. (b) The backward-looking PRISM view derived 45.3 s later than the nadir data of (a) shows the same area to the south of Nusa Penida (NP) and provides a similar depiction of internal waves. Selected surface currents (red) and internal-wave velocities (yellow) derived by the ATSSG technique have been drawn directly onto the image. W denotes weak internal-wave motion, whereas F marks the location of a weak front. Surface currents off the southeast corner of Nusa Penida (top right) indicate strong surface-current convergence toward the channel carrying the majority of the throughflow. The main internal-wave assemblage moves largely westward.

excellent Sun glitter impressions of internal waves propagating largely westward in the East Indian Ocean. In contrast, the forward-looking view provided somewhat poorer definition of these disturbances and hence these data have not been used in this study. Fig. 2 shows no indication of a brightness reversal of the type detected in ASTER data of Nam Co (Matthews et al., 2004) and demonstrates a close similarity between the nadir and backward-looking views. This impression is confirmed by a more detailed comparison of the data presented later in connection with Fig. 4. The correspondence is often closest at the trailing (rearward) edges of the internal waves, although variations may arise as a result of the factors discussed below. In line with earlier comments, we shall briefly discuss the imaging conditions relevant to the internal-wave signatures represented in the PRISM data of Fig. 2, while their oceanographic significance will be discussed elsewhere.

Internal waves such as these are imaged in Sun glitter when the powerful circulation systems they establish are able to influence the short-scale roughness characteristics of the sea surface. In practice this requires that the spatial gradients in surface current associated with the internal wave should be of a sufficient magnitude to effectively modulate the spectral energy densities of the short-gravity waves (and/or capillary waves) that are primarily responsible for the reflection of sunlight directly back to the spacecraft. The circumstances under which this condition is met, for both the nadir and backward-looking views shown in Fig. 2, can be examined in the normal way by considering the ambient Sun glitter radiance recorded at the sensor, $L_{sg,0}$, which is given to first order by the Cox and Munk (1954) relation as

$$L_{sg,0} = \left[\frac{H_{\odot}}{4\pi}\rho(\hat{\omega})\sec^4\hat{\beta}\sec\theta_v\right]\frac{1}{\sigma_0^2}\exp\left(-\frac{\tan^2\hat{\beta}}{\sigma_0^2}\right). \quad (1)$$

Here $H_{\odot}$ is the solar irradiance incident on the ocean surface, $\hat{\omega}$ is the incidence (or reflection) angle required for specular reflection of sunlight from a wave facet to the satellite, ρ is the Fresnel reflectivity, θ_v is the off-nadir viewing angle, $\hat{\beta}$ is the angle of tilt required for a surface facet to return light directly back to the sensor and σ_0^2 is the mean square slope of the water waves associated with the ambient surface conditions.

The first step in the analysis, following spatial co-registration of the two images, is to determine the cloud-height wind speed from the motion of cloud shadows over the ocean surface. This simple technique shows that, at the time of image acquisition, a southeasterly wind was blowing at about 2.5 m s^{-1}, consistent with meteorological expectation for this time of year. The parameter σ_0^2 appearing in Eq. (1) can then be estimated by using another of the Cox and Munk (1954) relations,

$$\sigma_0^2 = 0.003 + 0.00512 S_w \pm 0.004, \quad (2)$$

with S_w symbolizing the near-surface wind speed in m s^{-1}. This yields a maximum value of $\sigma_0^2 = 0.02$.

Next, the geometrical relations given in Matthews (2005) are used to calculate the values of the required tilt angles as $\hat{\beta} = 11.1°$ for the nadir case and $\hat{\beta} = 12.6°$ for the backward-looking case, with the sensor, orbital and solar parameters used in this calculation provided as supplementary information accompanying the image files. It is then a simple task to calculate radiances from Eq. (1). The resulting radiance curves for the nadir and back-looking cases are presented in Fig. 3. As indicated on this diagram, the ambient value of σ_0^2 (taken here as 0.02) is smaller than the values of $\tan^2\hat{\beta} = 0.038$ and $\tan^2\hat{\beta} = 0.05$ at which the maximum radiances for the two PRISM scenes occur (Melsheimer & Kwoh, 2001). This demonstrates that a brightness reversal of the type observed at Lake Nam Co (Matthews et al., 2004) should not be present in these data.

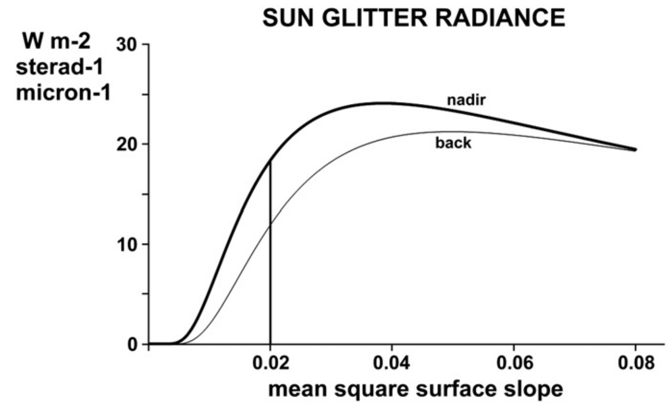

Fig. 3. Sun glitter radiance curve derived from Eq. (1) using parameter values relevant to the nadir and backward-looking PRISM images of the Lombok Strait region acquired on 26 September 2006. The vertical line drawn at the abscissa value of 0.02 denotes an ample estimate of the mean square surface slope associated with the prevailing wind conditions.

In the simplest interpretation, the similarity of the two radiance curves plotted in Fig. 3 implies that the action of an internal wave in locally enhancing or quenching the short scale surface roughness (and thereby influencing the "effective" value of mean square surface slope plotted along the abscissa of Fig. (3)) will produce comparable growth or suppression of the Sun glitter radiances within the two images. The internal-wave signatures should thus be alike in appearance, as a comparison of Fig. 2(a) and (b) indeed shows.

We note that the radiance values calculated here are substantially lower than those reported by Matthews et al. (2008) for ASTER Sun glitter data of Lake Nam Co. The latter were gathered under sensor and solar parameters that were excellent for Sun glitter imaging (with $\hat{\beta} = 5.41°$ for the ASTER near-nadir view), so that many subtle surface roughness features were revealed. In the case of the PRISM data of 26 September 2006, the imaging conditions were less favorable but were nevertheless adequate, owing to the fact that the mean square surface slope associated with the surface wind field ($\sigma_0^2 = 0.02$) lies on the "leading edge" of the radiance curve of Fig. 3, where the sensitivity to the perturbations induced by the internal wave is relatively high.

5. Synoptic mapping of internal-wave motions

In order to illustrate the basic principle of the differential technique used to deduce the vector motions of internal waves (and later of surface currents), we consider the small section of an internal wave that is encircled by the purple ring enclosed within the white rectangle of Fig. 2(a). Fig. 4(a) shows the nadir scene of this selected region while Fig. 4(b) gives the corresponding backward-looking view gathered 45.3 s later. Fig. 4(c) displays a composite image formed from these two scenes.

In Fig. 4(d), the nadir view is used to provide an underlying grayscale base image that has been brightness "flipped" in appearance (i.e. its look-up table has been inverted) so that bright regions of nadir Sun glitter appear dark. The time-delayed backward-looking view has then been overlaid onto this inverted nadir view, with most Sun glitter in this slant view represented in purple and with the brightest glitter features depicted in yellow. The small differential displacements caused by the slanted right-to-left motion of the internal wave over the 45.3 s period between the acquisition times of these two images cause a slight positional mismatch. This is apparent on the right-hand side of the image where the dark shadow-like regions of the underlying grayscale nadir image protrude from under the purple and yellow overlay. Measurement of the magnitude and orientation of the mean value of this displacement then enables the velocities of sections along the trailing edge of the internal wave to be determined

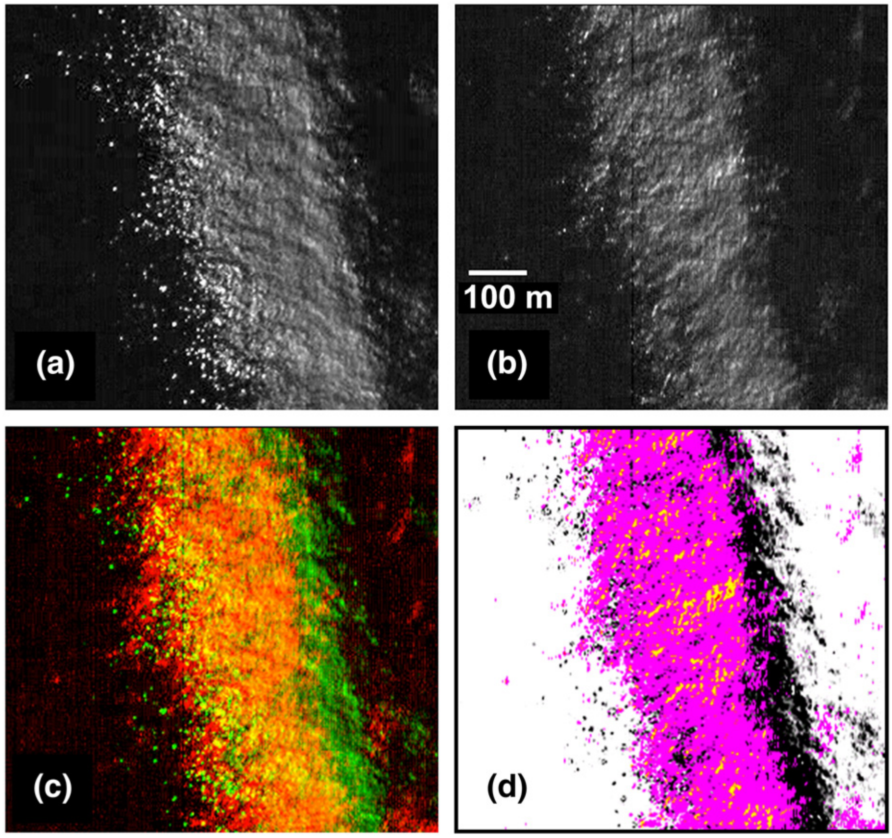

Fig. 4. Displays PRISM data from the region encircled by the purple ring in Fig. 2(a): (a) Shows the Sun glitter signature of an internal wave as gathered in the PRISM nadir view. Note the irregular speckle-like enhancement that is visible on the left side at the leading edge of the internal wave. (b) Displays data gathered from the corresponding backward-looking view. With no comparable speckle-like enhancement on the left, the internal-wave signature gives the appearance of being slightly narrower. (c) Provides a simple two-band composite image with the nadir view of (a) displayed in green and the later backward-looking view of (b) displayed in red. (d) Illustrates our preferred representation of displacement within the differential approach that forms the basis of the ATSSG technique. Here data from the backward-looking view (purple: raw pixel values from 46 to 60, yellow: >60) are overlaid onto an inverted version of the corresponding grayscale nadir view (raw pixel values >50 appear dark). The spatial displacement caused by the slanted right-to-left internal-wave motion over the time interval of 45.3 s between these two views is now clearly defined as a dark shadow-like overlap on the right-hand side, the average width of which corresponds to a speed of 1.6 m s^{-1}. The irregular speckle-like enhancement present at the leading edge of the internal wave within the nadir view does not consolidate into a comparable overlap region and has no influence on motion determinations made at the trailing edge.

(and yields an average speed of 1.6 m s^{-1} in the present case). Selected internal-wave velocity measurements derived in this way have been drawn onto Fig. 2(b) and are represented by yellow arrows.

Although the irregular speckle-like enhancement in Sun glitter radiance detected at the leading edge of the internal wave in the nadir view of Fig. 4(a) is not detected in the backward-looking view, this inter-view disparity has no impact on surface motion measurements made at the trailing edge in locations where the correspondence is relatively good. The speckle-like enhancement itself seems to represent a specific Sun glitter response to the energetic wave and current environment developing at the leading edges of these powerful internal waves and has attracted little if any attention in the published literature. It may also appear at leading edges in the backward-looking view and yet be absent from the nadir view, as Fig. 6(b) later shows, suggesting influences from both the viewing geometry and the wave orientation. Further work is required if the oceanographic significance of this feature is to be elucidated.

A synoptic view of internal-wave motions across a larger proportion of the internal-wave field than that represented in Fig. 4 is shown in Fig. 5 and covers the area within the white rectangle of Fig. 2(a). The propagation of a number of individual wave components can now be easily identified by their displacement "shadows" which, due to the roughly right-to-left internal-wave motion over the 45.3 s time period separating the two images, appear as thin black regions on the right-hand sides of the purple internal-wave features. Here again, the speckle-like enhancements at the leading edges (left sides) of the internal-waves in the nadir view have no influence on the motion deductions, as they do not consolidate into well-formed "shadow" regions. As far as the present authors are aware, the synoptic view depicted in Fig. 5 represents the first time that internal-wave motions developing over sub-minute timescales have been mapped across a broad disturbance field.

Note that the displacement "shadows" of individual internal-wave components (the widths of which are equivalent to local speed) are not uniform across the field of view. Hence, if good Sun glitter signatures can be captured in all three channels, a comparison of the forward-nadir and nadir-backward combinations might reveal the complex structural evolution of an internal-wave field at very high temporal and spatial resolutions.

6. Inter-view displacement and the change in viewing geometry

An alternative explanation of the origin of the Sun glitter displacements derived above in the application of the ATSSG technique is that they are generated as a direct result of the difference in observational geometry between the nadir to the backward-looking views, which would imply that the observed displacements are not truly indicative of the motion of the internal waves. This interpretation relies on our earlier conclusion that the slant view requires a new tilt angle for the surface facets engaged in the specular reflection of light back to the spacecraft and hence that the wave components responsible for the Sun glitter are different to those

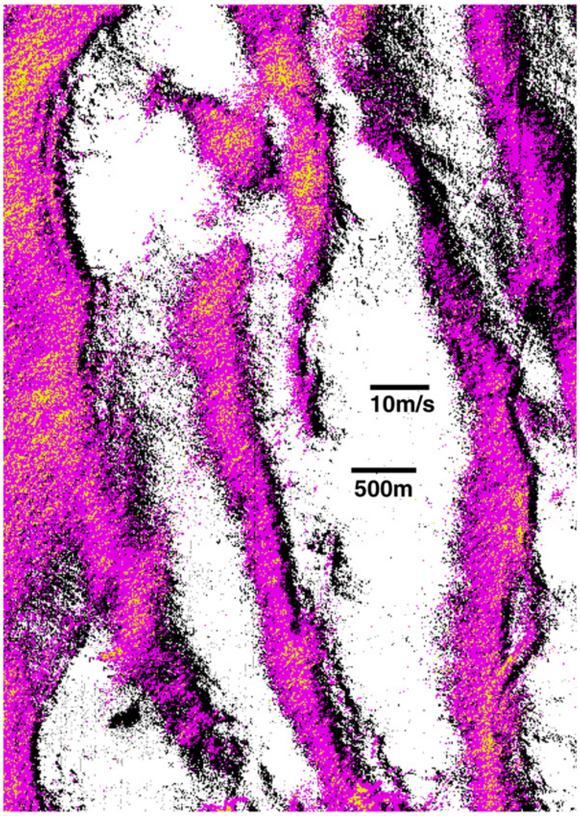

Fig. 5. A synoptic view of internal-wave motions detected within the region enclosed by the white rectangle of Fig. 2(a). As in Fig. 4(d), the grayscale look-up table of the underlying nadir base image has been inverted, so that the brightest features of the original data appear dark. The backward-looking view (purple and yellow, as in Fig. 4(d)) has then been overlaid onto this inverted nadir view. The differential displacements caused by the motions of the internal waves over the 45.3 s separating the nadir and backward-looking views appear as easily recognizable "shadows" in locations where the inter-view correspondence is good. Owing to the largely westward (right to left) propagation of the waves, the "shadows" appear on the right-hand sides of the internal waves. In contrast, on the left-hand sides, an effect from the irregular speckle-like variability discussed in connection with Fig. 4 is visible, but this does not form a consolidated "shadow" region so that the motion determinations remain unambiguous.

involved for the nadir view. If, for example, a spatial segregation of these two wave components is established within the surface region influenced by the internal wave, then separate zones of surface roughness would become highlighted within the two Sun glitter views, generating displacement "shadow" regions even if the internal wave is static. In this case we would expect essentially zero correspondence between the scattering elements that are active in the two views, as they would occupy wholly different locations.

The high-spatial and temporal resolutions of the PRISM Sun glitter data permit an investigation of this possible mechanism at an unprecedented level of detail. The data we use in this discussion are displayed in Fig. 6 and were extracted from a portion of the main invasive front of the internal-wave assemblage as denoted by the blue ring in Fig. 2(a).

The nadir and backward-looking views (Fig. 6(a) and (b) respectively) reveal an irregular, "frayed" profile of Sun glitter that defines the trailing edge of this internal-wave disturbance when viewed at the high 2.5-m spatial resolution of the PRISM sensor. As indicated by the numbers (running from 1 to 6), these two scenes exhibit a basic correspondence in terms of their fine structure, although it is apparent that this relation is far from precise. Rather, the backward-looking view depicts a "ghost" impression of the profile visible in the nadir view — one that has clearly evolved or has been otherwise reworked but yet retains recognizable structural similarities with the earlier nadir view. A similar level of loose correspondence is observed generally throughout these data and, though inexact, it nevertheless supports the notion of an advancing internal wave that activates a slowly evolving matrix of surface scattering elements. This in turn suggests that the inter-view displacements detected earlier are dictated primarily by the motions of specific scattering patterns that are intrinsic to the propagating internal-wave system, rather than by a spatial shift resulting simply from the change in imaging geometry.

To investigate these aspects in greater detail, the major component of the inter-view displacement, which we therefore take to reflect the propagation of the internal wave, has been removed from the backward-looking view across a straight portion of the trailing edge by a "bulk" matching of the main components of the Sun glitter profiles. The two views are then combined into a single composite image (Fig. 6(c)), which is shown at higher spatial resolution. The secondary (remnant) spatial discrepancies, now readily visible, seem to show no systematic trend or pattern, and thus indicate that the evolution of the internal-wave field over the 45.3 s between the two data takes probably overrides any influence from the change in viewing geometry. Crucially this shows that a bulk matching of the two Sun glitter signatures, based on the regions where the scattering elements are most densely packed, should produce a fairly robust means of determining the inter-view displacement associated with the propagation of the internal wave, since then the secondary displacements can be assumed to roughly cancel.

In a more general sense, if the inter-view displacements arise as a consequence of the change in imaging geometry alone then the internal-wave motions we derive would have a somewhat artificial nature — they would not necessarily be fastest at the main invasive front of the internal-wave system or slower in regions of internal-wave decay, or indeed would not radiate out appropriately from a known source region. Such expectations stand in contrast to the results displayed in Fig. 2. These conclusions may not, however, hold generally since the Lombok PRISM data represent a case in which the required tilt angle ($\hat{\beta}$) values are quite similar at 11.1° and 12.6° for the nadir and back-looking views respectively. Further investigation is required to determine whether the change in viewing geometry is more influential in situations where the required $\hat{\beta}$ tilt angles differ substantially between the two views.

7. The influences of slicks and swell waves

Other sources of inter-view displacement represent potentially serious impediments to the successful application of the ATSSG technique. The influences of slicks, surface gravity and swell waves, windrows, fronts and other phenomena were either absent or could be neglected in the data used for Figs. 4–6, since within the white rectangle of Fig. 2(a) conditions for motion detection were generally good. We now briefly present data gathered under somewhat less favorable conditions in an attempt to highlight difficulties that may arise in ATSSG-based assessment of internal-wave motions in a particular case when slick and swell-wave effects are present.

The data exhibited in Fig. 7 show the region enclosed by the green circle in Fig. 2(a). The relative positions of nadir points A and B of Fig. 7(a) and their co-located equivalents A′ and B′ in the backward-looking view of Fig. 7(b), give an immediate impression of the internal-wave motion. Points A and B also define a slick feature that moves relatively slowly toward the southwest. Note that, in line with the previous comments, this feature does not greatly change in appearance between the two views, as is best observed just below the center of the overlay image of Fig. 7(d), where the slick is represented by two adjacent tadpole-like features in white and black for the nadir and back-looking views, respectively. It is, however, noticeable that the slick is shorter in the backward-looking view below A′, since then the Sun glitter reduction due to the slick ceases entirely for reasons that

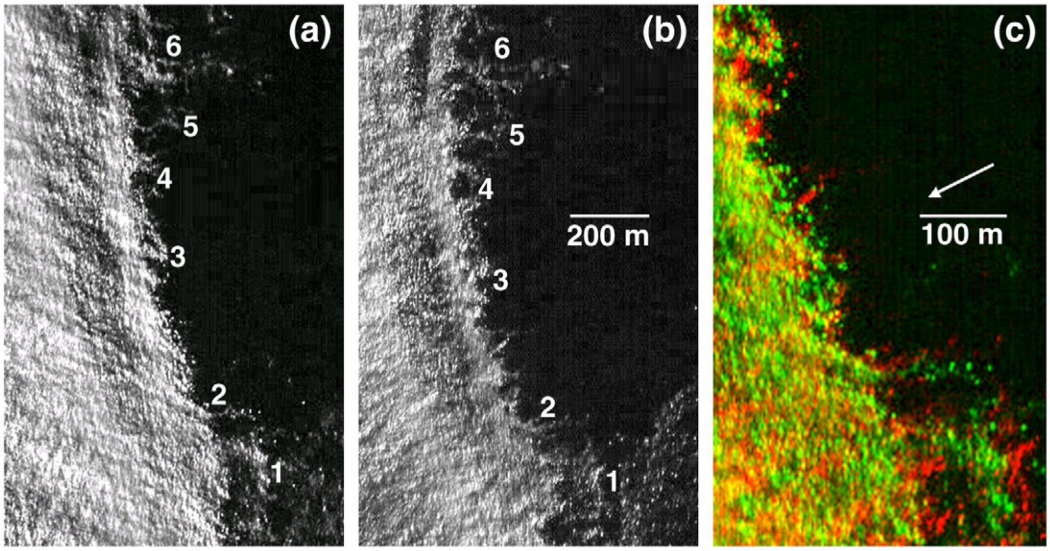

Fig. 6. Displays PRISM Sun glitter data from the region encircled by the blue ring in Fig. 2(a): (a) Shows the nadir view, in which the numbers 1–6 denote specific structural features formed along the trailing edge of the internal wave. (b) Gives the backward-looking view within the same spatial frame, with the numbers 1–6 used to denote corresponding structural features. Although the same basic substructure can be identified within the Sun glitter, the inter-view agreement is not precise. (c) Provides a two-band composite of the region enclosing features 1–3, with the nadir view represented in green and the motion-compensated backward-looking view in red. The white arrow, indicating the vector inter-view displacement used in the motion compensation, was obtained by matching the "bulk" components of the two Sun glitter signatures and corresponds to a local internal-wave speed of 1.8 m s^{-1}. A number of small inter-view discrepancies are visible that relate primarily to the evolution of the internal-wave field over the 45.3 s separating the two images, rather than to the change in viewing geometry.

are unclear. The presence of the slick in the "shadow" overlap region of Fig. 7(d) clearly restricts our ability to accurately gauge the local displacement caused by the motion of the internal wave.

A further adverse effect, and one that is potentially more serious, is due to swell waves. These latter are well represented in the nadir view of Fig. 7(a) and hence also influence Fig. 7(c) and (d). The wave component visible here represents a short swell of wavelength about 60 m that propagates diagonally across this section of the PRISM image and displays a northwest to southeast orientation. Fig. 7(d), in particular, shows how the swell acts to elongate the dark displacement region in an along-crest direction and thereby creates an irregular serrated border to the "shadow" zone from which it is difficult to obtain accurate estimates of the internal-wave phase speed. Fortunately, such adverse influences can generally be identified and avoided, although their presence underlines the need for caution in applications of the ATSSG method.

8. Surface-current determinations

The presence of slicks in Sun glitter images, though potentially injurious to attempts to measure the motions of internal waves, also has a positive aspect in that currents can be mapped by the ATSSG technique using the slicks as "passive" tracers of the surface motion of the water body. When such structures are clearly imaged in at least two of the data takes comprising the along-track stereo sequence, the same differential approach as employed above in the case of internal waves can be used. Consistent with our earlier comments in relation to the work of Jackson (2007), evidence obtained from experience to date indicates that ASTER and PRISM stereoscopic images of low-latitude coastal zones often exhibit the rich variety of "passive" tracers, in the form of slicks of both natural and anthropogenic origin, that is required to support the derivation of ATSSG currents in synoptic fashion. This is particularly the case when the images are gathered under low to moderate surface wind conditions. The selected surface-current determinations presented as supporting data in Fig. 2(b) (red arrows) provide relevant examples and were derived from the displacements of slicks that are often present in the Lombok Strait region. We note that Fig. 2(b) gives the first synoptic representation of simultaneous surface currents and internal-wave motions developing on sub-minute timescales and thus clearly demonstrates the diagnostic capability of the ATSSG technique.

A more comprehensive illustration of the capacity for surface-current determination is shown in Fig. 8. The data displayed here were obtained from the small region highlighted by the black star in Fig. 1 and represent a portion of an earlier PRISM frame gathered on 26 September 2006, acquired some 4 s before the data shown in Fig. 2. Here the images in the nadir view and back-looking view are very similar indeed (hence only nadir view shown) and their comparison readily yields surface motions. Since the surface-current fields vary smoothly, arrows have been used in Fig. 8 to represent selected displacement vectors that were, as above, deduced from the motions of the surface structures highlighted in the Sun glitter. The panel in the top left of Fig. 8 presents the zoomed profile of a "beaked" feature that is visible on the far right of the main diagram. The red line shows the displaced outline of this feature, as recorded 45.3 s later in the backward-looking view. The "passive" tracers (visible here as dark areas) may represent the moribund remnants of boat wakes, although natural oil seepage and local patches of enhanced biological activity are other potential sources of the surfactants responsible for such Sun glitter signatures.

The vectors shown in Fig. 8 indicate a region of strong current shear established at the time of data acquisition, when tidal conditions were evolving within the transition period from ebb to flood. Water depth decreases from about 400 m on the right (east) to about 100 m on the left of the image. The faster currents (up to 2.9 m s^{-1}) present in the deeper waters on the right are likely indicative of motion within the central channel, where the substantial monsoon-related residual flows are transported. Such rapid flows are consistent with earlier reports of strong currents with a magnitude of 3.5 m s^{-1} (Murray & Arief, 1988) recorded near the sill of the Lombok Strait, which lies further south between the islands of Nusa Penida and Lombok. The interesting aspect of these new data is that high surface-current values are also recorded well to the north of the sill.

Note that although the individual surface-current determinations made around the perimeter of a selected slick feature represented in the stereo sequence can, in principle, be made near the 2.5-m resolution of the sensor, this level of detail is not sustained across the whole field of view. Rather, the distribution of the surface roughness structures acting as passive tracers causes the velocity determinations

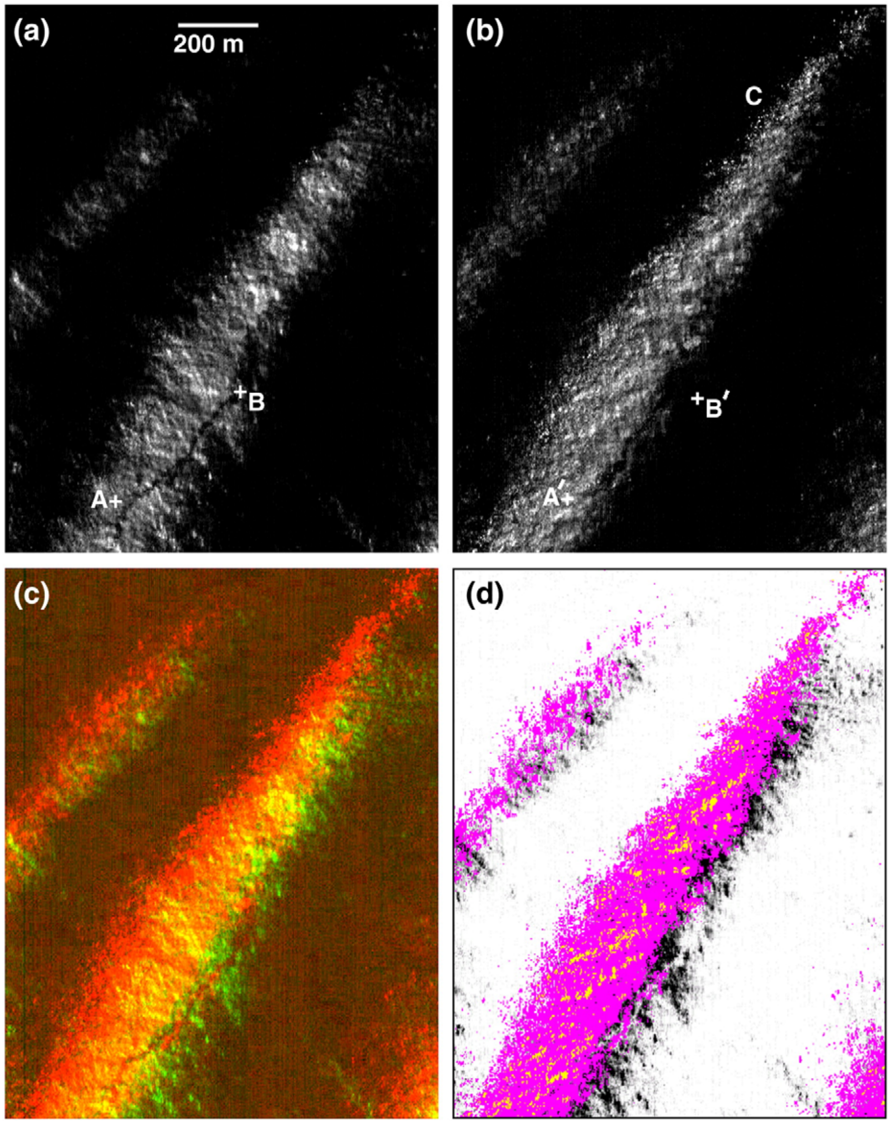

Fig. 7. Displays PRISM Sun glitter data from the region encircled by the green ring in Fig. 2(a): (a) Data acquired from the nadir view. Note the presence of a dark surface slick crossing the central region of the internal wave between points A and B (labeled in red) in which Sun glitter is suppressed due to the action of a surface film. (b) Data from the backward-looking view. Owing to the relatively rapid motion of the internal wave, the points A′ and B′ (in red), which represent the co-registered equivalents of the nadir points A and B, are clearly displaced toward the trailing edge of the internal wave. The label C marks an area of irregular speckle-like enhancement similar to that described in connection with the nadir view of Fig. 4(a). (c) Provides a two-band composite image with the nadir view of (a) displayed in green and the later backward-looking view of (b) displayed in red. (d) Shows data from the backward-looking view in purple and yellow overlaid onto an inverted version of the corresponding grayscale nadir view as in Fig. 4(d). In the lower center of the scene, the slick signatures resemble two adjacent tadpole-like features in white and black for the nadir and back-looking views, respectively, with the slick moving slowly to the southwest. The displacement "shadow", from which the internal-wave phase velocity can in principle be derived, is now distorted both by the presence of the slick and through the effect of swell waves detected principally in the nadir view. The latter propagate diagonally across the image with a northwest to southeast orientation and cause elongations to the "shadow" region in the along-crest direction.

to congregate into irregularly spaced clusters. Clearly, the dependence on an external source and the consequent reduction in effective spatial resolution produces a less satisfactory mapping than for internal waves (which generate their own Sun glitter signatures). This shortcoming is not, however, fatal for the success of the technique since, as stated above, there is often an abundance of workable "passive" surface roughness structures in Sun glitter images. By tracking the motion of these features, the ATSSG approach offers a means of fine-scale surface-current measurement that is presently unrivalled as a space-borne capability.

9. Other potential applications of the ATSSG method

A summary of potential aquatic applications of along-track stereo optical observations based on ASTER data has already been published (Matthews, 2005). Here we briefly highlight two further possibilities that arose during the course of our analysis of the September 2006 PRISM data of the Lombok Strait region.

Fig. 9 illustrates a complex scenario in which strong surface-gravity-wave refraction takes place at the main invasive front of the internal-wave assemblage recorded on 26 September 2006. The waves involved here are typically of a few tens of meters in wavelength and require, from a basic application of Snell's law (Kenyon, 1971), a transverse current of >1 m s^{-1} to effect their refraction. As outlined in Matthews (2005) for coastal swell, such data offer the potential for a highly detailed analysis of the wave propagation and surface-current regime in these poorly understood internal-wave dominated environments, particularly if the wave phase velocities can be derived by the ATSSG technique.

A similar untapped potential exists in the study of oceanic fronts, for which results obtained by detailed mapping of the frontal surface currents and wave-fields by the ATSSG method could play a useful

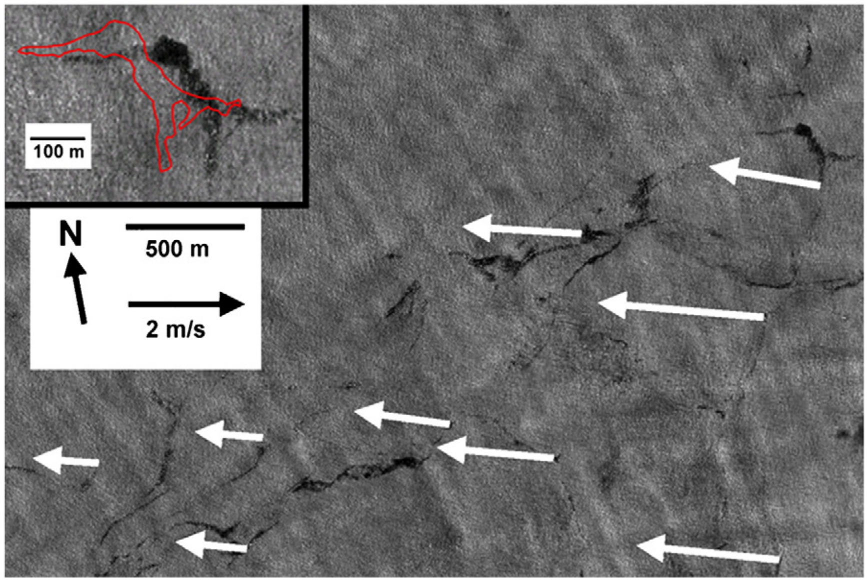

Fig. 8. Selected surface-current vectors determined by the ATSSG technique using PRISM Sun glitter data gathered at 02.41.05 UT on 26 September 2006 from the region marked by the star in Fig. 1. The inset panel in the top left shows a more detailed view of the "beaked" feature present on the far right of the main diagram. The displaced outline of this feature, as recorded 45.3 s later in the similar backward-looking view (not shown), is depicted by the red line, which encompasses data pixel values lying in the range between 40 and 45 (inclusive). Moribund remnants of boat wakes, natural oil seepage and locally enhanced biological activity are potential sources of the films responsible for the dark Sun glitter signatures visible here.

role in the development of theoretical models of frontogenesis and frontolysis. To briefly illustrate this area of application, Fig. 10(a) provides an overview of a weak front (labeled originally as F in Fig. 2(b)) of essentially unknown origin, which may possibly represent the moribund remnant of an earlier gyral structure formed off the interface between the rapid through-flow regime and relatively static waters of the Nusa Penida island wake.

In near-simultaneous surface temperature data gathered at 1.1 km spatial resolution by the NOAA-17 Advanced Very High Resolution Radiometer (data not shown), this frontal zone likely separates a region of cooler water (of temperature roughly 18 °C) in the west from water that is about two degrees warmer. Note that the clear definition of the frontal zone in both views enables the detailed motion of this boundary to be tracked, although here the front moves little between the two views. Given a broad distribution of slicks, it may be possible to map surface currents on both sides of such structures in order to investigate along-front flows and their related transverse convergences at high-spatial resolution.

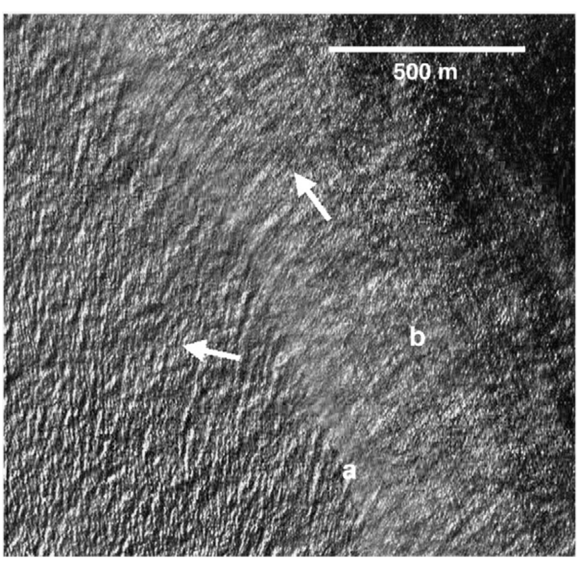

Fig. 9. Sun glitter variations recorded in the vicinity of the main invasive front of the internal-wave assemblage recorded by PRISM on 26 September 2006. The data are extracted from the bottom (left of center) of Fig. 2(b), in the backward-looking view. They show the refraction of surface gravity waves as indicated roughly by the direction change of the two white arrows, which is caused by a transverse near-surface current of magnitude >1 m s^{-1}. Feature "a" denotes modest enhancement in Sun glitter radiance at the main leading edge of the internal-wave system. Feature "b" denotes a region in which the surface gravity-wave component propagating normal to the leading edge becomes well defined within the region influenced by the refraction.

10. Summary and discussion

The ATSSG technique can support many applications in the monitoring of aquatic environments and is particularly well suited for research in spatially restricted areas typified by coastal zones, lakes, large rivers and sea straits such as the Lombok Strait. It is capable of providing useful information on the motions of internal waves, surface gravity and swell waves and fronts. Moreover, surface currents can be derived when "passive" tracers in the form of slicks are present. The method should provide a useful compliment to future all-weather SAR-based surface-current detection by offering an independent means of calibration and validation, since ATSSG-derived currents represent surface motions obtained directly from the measurement of a differential displacement over a fixed time interval and are not reliant on mechanical responses, heavy averaging or a specific interpretation of back-scattered radar spectra.

The major restriction inherent to the ATSSG approach stems from the requirement that Sun glitter must be present within at least two of the component images that make up the acquisition sequence of the along-track operation. This in turn implies that the solar and sensor orientations must be favorable, that cloud coverage should be sparse and that winds should be moderate or weak so that the surface roughness structures associated with internal waves, swell waves, slicks, fronts and other phenomena can be identified. Together, these instrumental and meteorological constraints create a more restrictive observational window than is commonly encountered with other visible-band or infrared remote sensing techniques. As a result, the opportunistic acquisition of Sun glitter data by topographic missions such as ASTER and PRISM takes place with relatively low regularity,

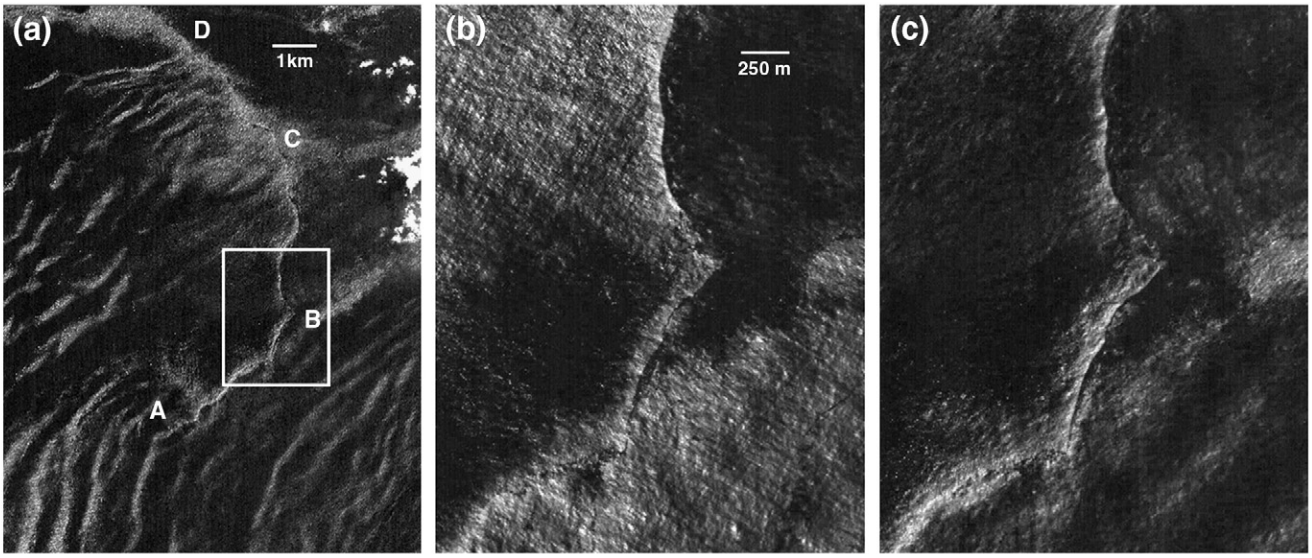

Fig. 10. (a) Shows Sun glitter variations recorded in the backward-looking view near the weak frontal region identified as F in Fig. 2(b). The letters ABCD define the front. The white rectangle encloses the region displayed in greater detail in Fig. 9(b) and (c). Note the disappearance of internal waves (propagating roughly from the southeast to northwest) as they encounter the frontal region and their subsequent reappearance further to the west. (b) Displays data from the nadir view gathered in the white rectangle of (a). (c) Shows the backward-looking view corresponding to (b). In principle, high-spatial resolution mapping of the surface currents developing in the frontal zone is possible when sufficient slick structures are present on both sides of the frontal boundary.

even during the summer months. Notwithstanding this unfavorable situation, much useful Sun glitter imagery continues to be collected, particularly at low latitudes, and many opportunities for internal wave and surface-current mapping arise. The present case study of dynamical phenomena in the Lombok Strait region illustrates this point.

With its higher spatial resolution and triplet viewing capability, PRISM offers a considerable improvement in performance relative to ASTER from the viewpoint of ATSSG accuracy. However, the greater tilt capability of the ASTER optical system allows a broader range of Sun glitter configurations to be investigated and the simultaneous surface temperature measurements made by ASTER facilitate the subsequent interpretation of the Sun glitter data, particularly when motions in the vicinity of frontal systems are under study. Future space-borne instrumentation would ideally combine the best features of the ASTER and PRISM missions by providing image triplets gathered at high-spatial resolution, adjustment of sensor view geometries to optimize the imaging of Sun glitter and simultaneous high-spatial resolution surface temperature sensing. In certain cases (as with the forward-looking sensor in the present study) Sun glitter is poorly defined in the slanted views and would require high-sensitivity imaging.

A number of factors determine the accuracy of motion determinations made using the stereo data gathered by these sensors. Of these, the requirement that Sun glitter features should remain congruent between the data takes within a stereo sequence requires some discussion. Clearly, if a specific zone of Sun glitter evolves greatly in shape over the time interval separating image pairs, then the motion determinations become suspect. In addition, if the slanted geometry of observation serves to highlight aspects of the surface roughness structure that are displaced spatially, then the possibility of error again arises. A consideration of these effects, at least for the data employed in this paper, led to the conclusion that a bulk matching of the main zones of Sun glitter enhancement generally provides a robust measure of the inter-view displacement and enables local internal-wave velocities to be derived.

The experience gained with these Lombok Strait PRISM data therefore indicates a basic compatibility between the Sun glitter signatures recorded within the nadir and backward-looking views, although this situation may be somewhat atypical in the sense that that the $\hat{\beta}$ values required in these two cases are quite similar. In contrast, near the northern limit of the Sun glitter regime (say at around 45° N in latitude), one might expect the nadir and forward-looking views of PRISM to provide the best Sun glitter representations and that the range of $\hat{\beta}$ values should be greater. Whether the comments and discussion presented here hold under these rather different conditions remains an open question.

In the absence of supporting *in situ* instrumentation or other means of motion detection by HF radar or SAR, it is difficult at this early stage to provide a fully rigorous analysis of the errors one might expect in ATSSG applications. Certainly, we recognize that discrepancies between image pairs of the type identified in Figs. 4 and 7 do not necessarily degrade the accuracy of the ATSSG technique, particularly if this is applied at the trailing edge of an internal wave and is preceded by a close inspection to identify malign influences. However, errors enter through a range of other sources such as from scene co-registration and irregularities related to minor misalignments in the optical configuration of the sensor (e.g. Kamiya, 2007), which are difficult to specify. Although crude estimates made so far indicate error levels of roughly 0.4 m s^{-1} in the derived internal-wave speeds, work is nevertheless underway to better define the errors involved in ATSSG-based motion determinations and will be reported in due course.

At present, practical application of the ATSSG technique makes use of fine spatial resolution Sun glitter imagery gathered as a serendipitous spin-off from terrestrial remote sensing programs. However, a dedicated program is required to fully exploit the potential of future high performance along-track optical sensors for observation of the hydrosphere using Sun glitter, and in particular for the determination of motions associated with internal waves, swell waves and surface currents. As the analysis of large volumes of Sun glitter data generated by such a program would be highly time consuming, some means of pattern recognition (a technique already employed in surface-current determination from temperature images by Turiel et al. (2008)) might prove helpful in identifying the motion of specific surface roughness structures within a stereo sequence. Although a dedicated space-borne Sun glitter sensor would improve our ability to monitor wave and surface-current regimes and would open a new chapter in oceanographic remote sensing, a number of practical problems must first be solved if it is to become a realistic prospect.

Acknowledgements

We wish to express our appreciation to staff and colleagues of the Department of Geophysics, Kyoto University, Japan, and in particular to K. Ishikawa and M. Konda, for their continuing support. We also thank S. Masuda and other staff of the Frontier Research Program at the Japan Marine Science and Technology Center (JAMSTEC) and acknowledge support from S. Shima. We owe a debt gratitude to staff from the Japan Aerospace Exploration Agency (JAXA) and the National Aeronautics and Space Administration (NASA) for their work in the development of the ASTER and PRISM sensors. PRISM images were obtained from the Remote Sensing and Technology Center (RESTEC) of Japan, while ASTER scenes were obtained from the Japanese Earth Remote Sensing and Data Acquisition Center (ERSDAC). The excellent libraries and computing services of the Universities of Kyoto, Japan and Bangor, Wales provided essential support during the compilation of this paper. In this latter respect we thank C. Jago, J. Davies and M. Duggan. The manuscript was improved on the basis of helpful comments provided by two referees.

References

Alford, M. H. (2003). Redistribution of energy available for ocean mixing by long-range propagation of internal waves. *Nature*, *423*, 159−162.

Apel, J. R., Byrne, H. M., Proni, J. R., & Charnell, R. L. (1975). Observation of oceanic internal and surface waves from the Earth Resources Technology Satellite. *Journal of Geophysical Research*, *80*, 865−881.

Arief, D., & Murray, S. P. (1996). Low frequency fluctuations in the Indonesian throughflow through Lombok Strait. *Journal of Geophysical Research*, *101*(C5), 12,455−12,464.

Barrick, D. E., Evans, M. W., & Weber, B. L. (1977). Ocean surface currents mapped by radar. *Science*, *198*(4313), 138−144.

Chapron, B., Collard, F., & Ardhuin, F. (2005). Direct measurements of ocean surface velocity from space: Interpretation and validation. *Journal of Geophysical Research*, *110*, C07008. doi:10.1029/2004JC002809.

Chong, J. C., Sprintall, J., Hautala, S., Morawitz, W. L., Bray, N. A., & Pandoe, W. (2000). Shallow throughflow variability in the outflow straits of Indonesia. *Geophysical Research Letters*, *27*(1), 125−128.

Cox, C., & Munk, W. (1954). Measurement of the roughness of the sea surface from photographs of the Sun's glitter. *Journal of the Optical Society of America*, *44*(11), 838−850.

Fu, L., & Chelton, D. B. (1985). Observing large-scale temporal variability of ocean currents by satellite altimetry. *Journal of Geophysical Research*, *90*(3), 4721−4739.

Garrett, C., & Munk, W. (1979). Internal waves in the ocean. *Annual Review of Fluid Mechanics*, *11*, 339−369.

Goldstein, R. M., & Zebker, H. A. (1987). Interferometric radar measuement of ocean surface currents. *Nature*, *328*, 707−709.

Gordon, A. L. (2005). Oceanography of the Indonesian seas and their throughflow. *Oceanography*, *18*(4), 14−27.

Haury, L. R., Briscoe, M. G., & Orr, M. H. (1979). Tidally generated internal wave packets in Massachusetts Bay. *Nature*, *278*, 312−317.

Hennings, I., Matthews, J. P., & Metzner, M. (1994). Sun glitter radiance and radar cross-section modulations of the sea bed. *Journal of Geophysical Research*, *99*(C8), 16303−16326.

Igarashi, T. (2001). ALOS mission requirement and sensor specifications. *Advances in Space Research*, *28*(1), 127−131. doi:10.1016/SO273-1177(01)00316-7.

Jackson, C. (2007). Internal wave detection using the Moderate Resolution Imaging Spectroradiometer (MODIS). *Journal of Geophysical Research*, *112*, C11012. doi:10.1029/2007JC004220.

Johannessen, J. A., Chapron, B., Collard, F., Kudryavtsev, V., Mouche, A., Akimov, D., et al. (2008). Direct ocean surface velocity measurements from space: Improved quantitative interpretation of Envisat ASAR observations. *Geophysical Research Letters*, *35*, L22608. doi:10.1029/2008GL035709.

Kamiya, I. (2007). Geometric characteristics of the early products of ALOS PRISM. *Bulletin of the Geographical Survey Institute of Japan*, *54*, 75−82.

Kenyon, K. E. (1971). Wave refraction in ocean currents. *Deep-Sea Research*, *18*, 1023−1034.

Klein, P., Isern-Fontanet, J., Lapeyre, G., Roullet, G., Danioux, E., Chapron, B., et al. (2009). Diagnosis of vertical velocities in the upper ocean from high resolution sea surface height. *Geophysical Research Letters*, *36*, L12603. doi:10.1029/2009GL038359.

Matthews, J. P. (2005). Stereo observations of lakes and coastal zones using ASTER imagery. *Remote Sensing of Environment*, *99*, 16−30. doi:10.1016/j.rse.2005.04.029.

Matthews, J. P., Fox, A. D., & Prandle, D. (1993). Radar observations of an along-front jet and transverse flow convergence associated with a North Sea front. *Continental Shelf Research*, *13*(1), 109−130.

Matthews, J. P., Wallis, S. R., & Yamaguchi, Y. (2004). ASTER views a high altitude Tibetan lake in stereo. *EOS*, *85*(43), 435.

Matthews, J. P., Wismann, V., Lwiza, K., Romeiser, R., Hennings, I., & de Loor, G. P. (1997). The observation of the surface roughness characteristics of the Rhine plume frontal boundaries by simultaneous Airborne Thematic Mapper and multifrequency helicopter-borne radar scatterometer. *International Journal of Remote Sensing*, *18*(9), 2021−2033.

Matthews, J. P., Yang, X. -D., Shen, J., & Awaji, T. (2008). Structured Sun glitter in an ASTER along-track stereo image of Nam Co Lake (Tibet): An interpretation based on supercritical flow over a lake floor depression. *Journal of Geophysical Research*, *113*, C01019. doi:10.1029/2007JC004204.

Melsheimer, C. and Kwoh, L. K. (2001). Sun glitter in SPOT images and the visibility of oceanic phenomena. *Paper presented at the 22nd Asian Conference on Remote Sensing, 5–9 November 2001, Singapore*.

Meyers, G. (1996). Variation of Indonesian throughflow and the El Niño-Southern Oscillation. *Journal of Geophysical Research*, *101*(C5), 12,255−12,263.

Mitnik, L., Alpers, W., & Hock, L. (2000). Thermal plumes and internal solitary waves generated in the Lombok Strait studied by ERS SAR. *ERS-Envisat Symposium: Looking down to Earth in the New Millennium 16–20 October 200. Gothenburg, Sweden. SP-461* (pp. 1−9). Noordwijk, The Netherlands: European Space Agency Publication Division.

Munk, W., Armi, L., Fischer, K., & Zachariasen, F. (2000). Spirals on the sea. *Proceedings of the Royal Society of London, Series A*(456), 1217−1280.

Murray, S. P., & Arief, D. (1988). Throughflow into the Indian Ocean through the Lombok Strait, January 1985–January 1986. *Nature*, *333*, 445−447.

Ponte, R. M., & Quinn, K. J. (2009). Bottom pressure changes around Antarctica and wind-driven meridional flows. *Geophysical Research Letters*, *36*, L13604. doi:10.1029/2009GL039060.

Prandle, D., & Matthews, J. P. (1990). The dynamics of nearshore surface currents generated by tides, wind and horizontal density gradients. *Continental Shelf Research*, *10*(7), 665−681.

Romeiser, R., Breit, H., Eineder, M., Runge, H., Flament, P., de Jong, K., et al. (2005). Current measurements by SAR along-track interferometry from a space shuttle. *IEEE Transactions on Geoscience and Remote Sensing*, *43*(10), 2315−2324.

Romeiser, R., & Runge, H. (2007). Theoretical evaluation of several possible along-track InSAR modes of TerraSAR-X for ocean current measurements. *IEEE Transactions on Geoscience and Remote Sensing*, *45*(1), 21−35.

Romeiser, R., Runge, H., Suchandt, S., Sprenger, J., Weilbeer, H., Sohrmann, A., et al. (2007). Current measurements in rivers by spaceborne along-track InSAR. *IEEE Transactions on Geoscience and Remote Sensing*, *45*(12), 4019−4031.

Sprintall, J., Wijffels, S., Gordon, A. L., Ffield, A., Molcard, R., Dwi Susanto, R., et al. (2004). INSTANT: A new international array to measure the Indonesian throughflow.*EOS*, *85*(39) 369 and 376.

Sprintall, J., Wijffels, S. E., Molcard, R., & Jaya, I. (2009). Direct estimates of the Indonesian throughflow entering the Indian Ocean: 2004–2006. *Journal of Geophysical Research*, *114*, C07001. doi:10.1029/2008JC005257.

Susanto, R. D., Mitnik, L., & Zheng, Q. (2005). Ocean internal waves observed in the Lombok Strait. *Oceanography*, *18*(4), 80−87.

Turiel, A., Solé, J., Nieves, V., Ballabrera-Poy, J., & Garcia-Ladona, E. (2008). Tracking ocean currents by singularity analysis of microwave sea surface temperature images. *Remote Sensing of Environment*, *112*(5), 2246−2260.

Wunsch, C., & Ferrari, R. (2004). Vertical mixing, energy, and the general circulation of the oceans. *Annual Review of Fluid Mechanics*, *36*, 281−314.

Wyrtki, K. (1987). Indonesian through flow and the associated pressure gradient. *Journal of Geophysical Research*, *92*(C12), 12941−12946.

Yoshikawa, Y., & Masuda, A. (2009). Seasonal variations in the speed factor and deflection angle of the wind-driven surface flow in the Tsushima Strait. *Journal of Geophysical Research*, *114*, C12022. doi:10.1029/2009JC005632.

Zhang, K., Douglas, B. C., & Leatherman, S. P. (2004). Global warming and coastal erosion. *Climatic Change*, *64*(1–2), 41−58. doi:10.1023/B:CLIM0000024690.32682.48.

Zhao, Y., Liu, A. K., & Hsu, M. -K. (2008). Internal wave refraction observed from sequential satellite images. *International Journal of Remote Sensing*, *29*(21), 6381−6390.